ISBN: 978-3-95450-227-1 ISSN: 2673-5490 doi:10.18429/JACoW-IPAC2022-WEOZSP3

MEASUREMENTS OF RADIATION FIELDS FROM A CERAMIC BREAK

Y. Shobuda, T. Toyama, M. Yoshimoto, S. Hatakeyama
J-PARC Center, JAEA/KEK, Ibaraki, Japan

Abstract

Ceramic breaks are used in synchrotrons for many purposes. For example, they are inserted between the Multi-Wire Profile Monitor (MWPM) on the injection line at the Rapid Cycling Synchrotron (RCS) in J-PARC to completely prevent the wall currents accompanying beams from affecting the MWPM. On the other hand, from the viewpoint of suppressing beam impedances and the radiation fields from the ceramic breaks, it would be preferable that the inner surface of the ceramic break is coated with Titanium Nitride (TiN), or covered over capacitors. In this report, we measure the radiation fields from the ceramic break with and without capacitors as well as the beam profile and investigate the effect of the ceramic breaks on the measurements.

INTRODUCTION

The RCS in J-PARC [1] has been realizing the high-intensity beams [2–4] by accumulating H^- injection beams from the LINAC. During the injection painting process [5], the H^- beams are transformed into the proton beams after being hit on the foil at the injection point. When two bunched beams, each containing 4.15×10^{13} particles per bunch, are accelerated from 400 MeV to 3 GeV at a repetition rate of 25 Hz, a 1 MW beam can be performed at the RCS.

Precise adjustment of the injection beams on the phase space area during the painting process is important to realize the high intensity beams with low beam loss rate. Hence, seven MWPMs [6] are installed, where MWPM1 is on the injection line to the RCS, MWPM2-5 are on the merging area in the RCS, and MWPM6-7 are on the dump line to measure the unstripped H^- beams. Based on the design concept of RCS, MWPM1 is sandwiched by two ceramic breaks to completely prevent the wall currents with H^- beams from interfering with the measurements with MWPM1 (see Fig. 1).

On the other hand, suppressing beam coupling impedances [7, 8] is a critical issue to accomplish high intensity beams. Since the impedance of ceramic breaks is closely related to the radiations from the ceramic break [9–13], covering capacitors on the ceramic breaks is an effective way to suppress both the impedance and radiations from the ceramic breaks. Therefore, it is important to directly measure the radiations from several types of ceramic break, and investigate the effects of ceramic breaks on the monitors.

The MWPM1 and the ceramic breaks next to it are good tools because the residual dose around there is kept below at most ten micro-sievert per hour even after 4 hours of 830 kW beam operation stop of the RCS. In this report, we measure the radiations from 15 mm long ceramic break with 101 mm inner and 111 mm outer radii beside MWPM1 by which the transverse beam profile is measured under several conditions, after test-measuring the magnetic field in the electromagnetic anechoic chamber in JAXA [14].

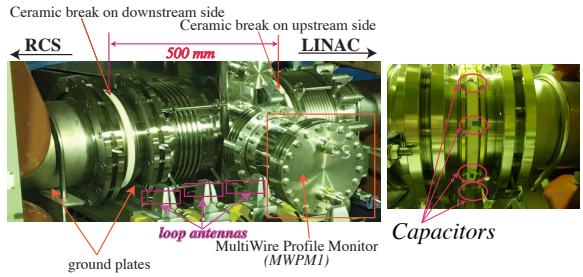

Figure 1: MWPM1 and the ceramic breaks without (left) and with capacitors (right).

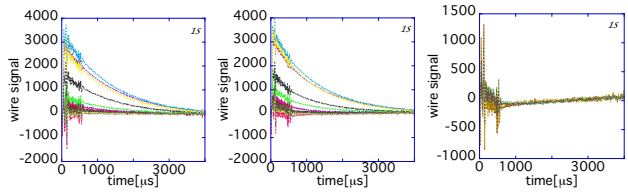

Figure 2: Signals if the ceramic break is covered by capacitors (left), or by Al with (center) and without beams (right).

MEASUREMENTS OF THE TRANSVERSE BEAM PROFILE

MWPM1 consisting of 27 wires measures the transverse beam profile in u and v axes, which are tilted 45° from the horizontal and vertical axes. Each wire moves 0.1 mm/s filling the intervals of respective wires, while 100 LINAC beams pass there with a 1 Hz repetition rate [6]. The integration of respective wire signals over 4 ms after being excited by a hit of the beam provides the beam density at the wire positions, so that a smooth bunch distribution is obtained after 100 LINAC beam shots.

Here, let us cover the ceramic break on the downstream side by twelve 1μF capacitors [15] with 2 MHz resonant frequency or by Aluminum (Al) sheet to investigate the effects on the beam profiles. The measured 27 wire signals are shown in Fig. 2. We can identify the noise from 0 to 0.7 ms in both cases (left/center). Though the capacitors are expected to suppress the low-frequency components of currents, high-frequency components contribute to the noise. This is a systematic error by the trapezoid bump magnets [16] at the injection area on the RCS rather than the wall currents with beams because it is excited even in the case without beams (see the right). As a result, it can be eliminated in principle to produce the smooth beam profiles.

ISBN: 978-3-95450-227-1 ISSN: 2673-5490 doi:10.18429/JACoW-IPAC2022-WEOZSP3

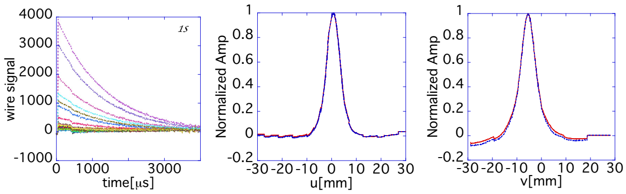

Figure 3: Wire signals (left) and beam profiles (center/right).

Finally, we have identified that the noise is excited through the ground plates in Fig. 1. After the plates are removed, the error diminishes on the signals even when the downstream and upstream ceramics are covered over capacitors and Al, respectively, as shown in the left panel of Fig. 3, and no integration gate dependence is found in the produced distribution in the center/right figures, where the red and blue lines are obtained by setting the integration gates over 0-4 ms and 0.7-4 ms on the signals, respectively. The identification of the noise path enables the capacitors to perfectly suppress the adverse effect on the monitors from the nearby magnets.

MEASUREMENTS OF RADIATIONS

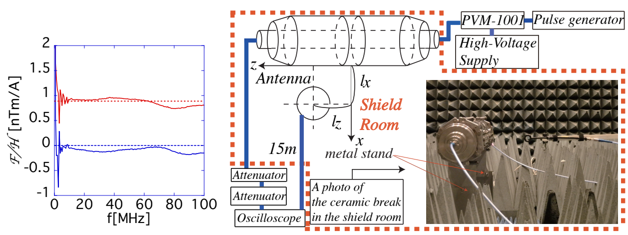

Figure 4: The frequency dependence of measured magnetic flux (left), and the measurement setup including a photo of the ceramic break in the shield room in JAXA (right).

Now, let us investigate whether the capacitors can suppress the radiation around the ceramic break beside MWPM1, after measuring the magnetic fields from a 10 mm long ceramic break with and without TiN coating in the electromagnetic anechoic chamber in JAXA by using a 30 mm diameter loop antenna [17] whose upper resonant frequency is 1.5 GHz. The left figure of Fig. 4 shows the frequency dependence of measured magnetic flux divided by the magnetic field at the center of the loop. The red and blue lines show the real and imaginary parts, while the dashed lines show the calculated theoretical results [18].

The right figure of Fig. 4 shows a schematic of the measurement setup and a photo of the ceramic break in the shield room in JAXA, where the ceramic breaks are supported by the metal stand ensuring the ground path for the wall current [11]. The ceramic breaks were sandwiched between two stainless-steel chambers. The inner conductor was placed in the center of chambers, making a coaxial structure with 50 Ω characteristic impedance. The upstream side was connected to the pulse generator [19], which was amplified up to 1 kV by the pulse voltage module (PVM-1001 [20]). We generated a pulse with a rise time of 5 ns and a fall time of 5 ns with a flat top time of 60 ns. The port on the downstream side and the antenna were connected to an oscilloscope [21] via 40 dB attenuator [22], and 15m coaxial cable [23], respectively. The position of the antenna is specified by $(l_x, 0, l_z)$ in the right figure. By rotating the antenna, we measured the magnetic flux in the longitudinal and vertical directions.

Figure 5 shows the simulations by CST [24] and 300 time averaged measurements. The upper-center/right and the other panels show the signals at the downstream port and magnetic fields at $(l_x, 0, l_z)$, respectively. The simulations for metal are calculated after the ceramic break is replaced with a perfectly conductive (PEC) pipe. The measured magnetic field is obtained after integrating the measured induced voltage on the antenna over time under the assumption that the magnetic flux is constant in the loop. The upper-center/right panels illustrate the modulated pulses monitored at the downstream port due to the impedance mismatch, which is significant for the ceramic break without TiN coating. The input pulse of simulation is 100 times lower than that of measurement, making both results of radiations different by 2 orders, sustaining both output pulses in the same order. The simulations and measurements are in agreement except in the case where the antenna is positioned at (200 mm, 0, 0), which means that the uniformity of the magnetic flux on the antenna is significantly violated in the loop. Hence, the antennas are placed at (270 mm, 0, 0) even in the nearest position at the following measurements in the RCS. The measured purple solid and brown dashed lines are almost identical and only the vertical component H_y is excited under this idealistic environment, as suggested by the simulation and theory [13]. Moreover, the measurements demonstrate that the magnetic field is significantly shielded by TiN coating with 10 nm thickness as expected [9–12].

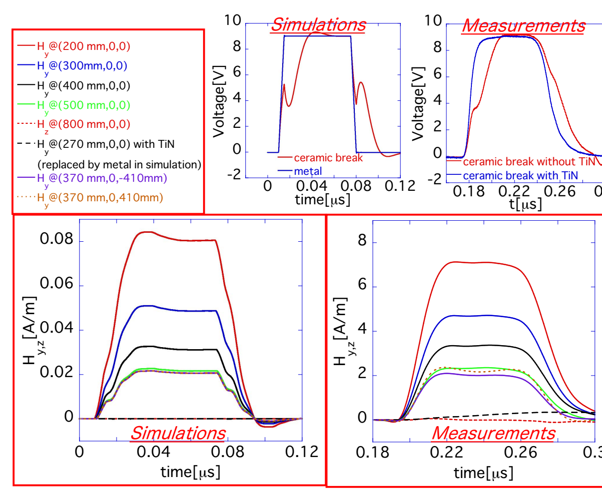

Figure 5: Simulations and measurements.

Now, let us measure the radiation from the ceramic break when H^- beam with $\beta = 0.7$, 90 ns width, and -4.45 nC passes through it in the RCS. The longitudinal beam shape

ISBN: 978-3-95450-227-1 ISSN: 2673-5490 doi:10.18429/JACoW-IPAC2022-WEOZSP3

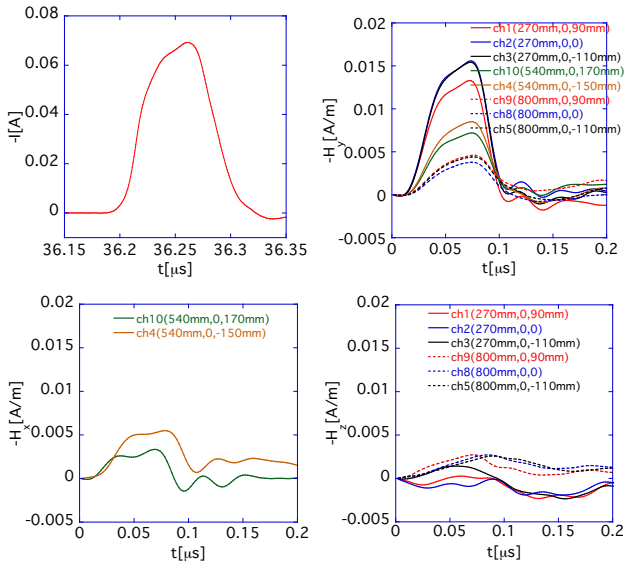

Figure 6: The observed wall current (upper-left) and magnetic fields (the others) from the ceramic breaks, which are averaged over 256 times.

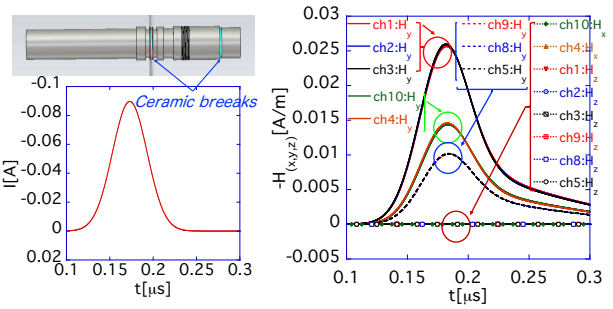

Figure 7: The simulation setup (upper-left), the input beam (lower-left), and the simulated magnetic fields (right).

is measured by a wall current monitor to be confirmed. The positions of eight antennas are identified by [**ch1** (270 mm, 0, 90 mm), **ch2** (270 mm, 0, 0 mm), **ch3** (270 mm, 0, −110 mm)], [**ch10** (540 mm, 0, 170 mm), **ch4** (540 mm, 0, −150 mm)], and [**ch9** (800 mm, 0, 90 mm), **ch8** (800 mm, 0, 0 mm), **ch5** (800 mm, 0, −110 mm)], where (**ch1**, **ch3**), (**ch10**, **ch4**), and (**ch9**, **ch5**) are almost symmetric for $z = 0$ plane.

Figures 6 and 7 show the measurements and simulations without capacitors neither TiN coating. Compared to the test-stand case, the situation is too complicated to perform accurate simulations from viewpoints of modeling the real environment. Then, the simulation setup is simplified as in the left panel of Fig. 7. Nonetheless of the simplification, the results feature the measurements, because H_y partially reflects the longitudinal bunch shape, is almost symmetric for the $z = 0$ plane, and systematically decreases as l_x increases in both the simulations and measurements. The shape distortion may be found by more precisely observing the tail part of H_y. Though the simulation suggests the radiations should not be emitted in the longitudinal and horizontal directions,

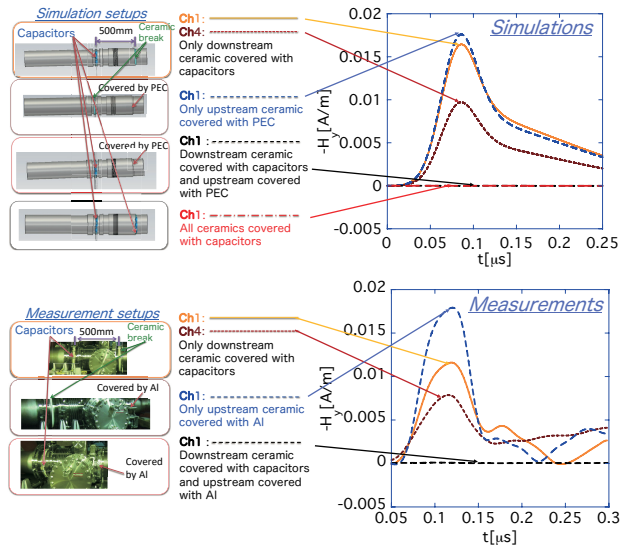

Figure 8: The simulation and measurement setups (left), simulated and measured magnetic fields (right) at **ch1** (270 mm, 0, 90 mm) and **ch4** (540 mm, 0, −150 mm).

they are produced in the measurements owing to the objects in J-PARC. One drawback of this simplified simulation is that the results are 1.5 times larger than the measurements, which may be improved by modifying the input pulse shape.

Now, let us simulate two cases, where the capacitors are attached to the downstream only, or PEC is covered over the upstream only. As shown in Fig. 8, the simulations suggest the radiations from both ceramics can be comparable at **ch1**, although the distances from the downstream and the upstream to **ch1** are 285 mm and 650 mm, respectively. The corresponding measurements at **ch1** reveal the contribution from upstream is not negligible. Hence, let us compare the results of **ch1** with **ch4**, where the distances from the 'upstream' ceramic breaks to **ch1** and **ch4** are both 650 mm, when the capacitors are attached only to the 'downstream' ceramic break because theoretical results predict that the magnetic fields are enhanced near the chamber wall [13]. Both the simulations and measurements demonstrate the enhancement, nonetheless of the existence of MWPM1.

To cure the situation, let us cover the upstream ceramic break with Al sheet (or capacitors) as well as the downstream one with capacitors, as shown in Fig. 8. The simulations and measurements in Fig. 8 demonstrate the remarkable suppression of the radiations. Practically, the ceramic break with 10 nm thin TiN coating can be more beneficial because the induced voltage on the ceramic break can provide the precise bunch shapes [11], suppressing the radiations.

SUMMARY

Since the chamber walls significantly enhance the magnetic field from the ceramic breaks, simplified simulations are effective to evaluate it when the ceramic breaks are close to monitors. The noise stemming from the ground should be carefully investigated when we cure the ceramic breaks.

This work was supported by KAKENHI (17K05124).

ISBN: 978-3-95450-227-1 ISSN: 2673-5490 doi:10.18429/JACoW-IPAC2022-WEOZSP3

REFERENCES

[1] Japan Accelerator Research Complex, https://j-parc.jp/c/en/index.html

[2] H. Hotchi *et al*, 'Achievement of a low-loss 1-MW beam operation in the 3-GeV rapid cycling synchrotron of the Japan Proton Accelerator Research Complex", *Phys. Rev. Accel. Beams*, vol. 20, p. 060402, 2017, https://doi.org/10.1103/PhysRevAccelBeams.20.060402

[3] H. Hotchi *et al.*, "Realizing a High-Intensity Low-Emittance Beam in the J-PARC 3-GeV RCS", in *Proc. IPAC'17*, Copenhagen, Denmark, May 2017, pp. 2470–2473. doi:10.18429/JACoW-IPAC2017-WEOAA3

[4] H. Hotchi *et al*, "Realizing a high-intensity low-emittance beam in the J-PARC 3-GeV RCS", *Journal of Physics: Conference Series*, vol. 874, p. 012059, 2017. https://doi.org/10.1088/1742-6596/874/1/012059

[5] P. K. Saha *et al*, "Direct observation of the phase space footprint of a painting injection in the Rapid Cycling Synchrotron at the Japan Proton Accelerator Research Complex", *Phys. Rev. ST Accel. and Beams*, vol. 12, p. 040403, 2009. https://doi.org/10.1103/PhysRevSTAB.12.040403

[6] S. Hatakeyama *et al*, "Development of Data Acquisition System of J-PARC RCS Multi-Wire Profile Monitor using Multi-Channel Digitizer", in *Proceedings of the 10th Annual Meeting of Particle Accelerator Society of Japan*, Nagoya, Japan, Aug 2013, p. 1082. https://pasj.jp/web_publish/pasj10/proceedings/PDF/SUP0/SUP074.pdf

[7] A. W. Chao, *Physics of collective beam instabilities in high energy accelerators*, Wiley, New York, 1993.

[8] B. W. Zotter *et al*, *Impedances and wakes in high-energy particle accelerators*, World Scientific, Singapore, 1998.

[9] Y. Shobuda *et al*, "Coupling impedances of a resistive insert in a vacuum chamber", *Phys. Rev. Spec. Top. Accel Beams*, vol. 12, p. 094401, 2009. https://doi.org/10.1103/PhysRevSTAB.12.094401

[10] Y. Shobuda *et al*, "Impedance of a ceramic break and its resonance structures ", *Phys. Rev. Spec. Top. Accel Beams*, vol. 17, p. 091001, 2014 https://doi.org/10.1103/PhysRevSTAB.17.091001

[11] Y. Shobuda *et al*, "Titanium nitride-coated ceramic break for wall current monitors with an improved broadband frequency response", *Phys. Rev. Accel. Beams*, vol. 23, p. 092801, 2020. https://doi.org/10.1103/PhysRevAccelBeams.23.092801

[12] Y. Shobuda, "Two-dimensional resistive-wall impedance with finite thickness: its mathematical structures and their physical meanings", *Progress of Theoretical and Experimental Physics*, vol. 2022, no. 5, 2022. https://doi.org/10.1093/ptep/ptac053

[13] Y. Shobuda *et al*, "Coupling impedances of a gap in vacuum chamber", *Phys. Rev. Spec. Top. Accel Beams*, vol. 10, p. 044403, 2007. https://doi.org/10.1103/PhysRevSTAB.10.044403

[14] Japan Aerospace Exploration Agency, https://global.jaxa.jp/

[15] Murata, https://www.murata.com/en-us/products/productdetail?partno=RCER72E105K5B1H03B

[16] Y. Shobuda *et al*, "Analytical method for the evaluation of field modulation inside the rf-shielded chamber with a time-dependent dipole magnetic field", *Phys. Rev. Spec. Top. Accel Beams*, vol. 12, p. 032401, 2009. https://doi.org/10.1103/PhysRevSTAB.12.032401

[17] ETS·Lindgren, 7405 E & H Near Field Probe Set, https://www.ets-lindgren.com/products/probes-monitors/eh-near-field-probe-sets/9004/900401?page=Products-Item-Page

[18] G. S. Smith, "Loop antennas", R. C. Johnson & H. Jasik (Editors), *Antenna Engineering Handbook*, Chapter 5, McGraw-Hill, NY, 3rd Ed., 1993

[19] Tektronix, KEITHLEY 3390 50MHz Arbitrary Waveform Generator, https://www.tek.com/

[20] BNC DEI High Voltage, PVM-1001-P +950V 10ns OEM Pulse Generator Module, https://directedenergy.com/product/pvm-1001-p/

[21] Teledyne Lecroy, WavePro 715Zi-A, https://teledynelecroy.com

[22] Tamagawa Electronics Co. Ltd, UFA-100NPJ-20, http://www.tmele.jp/english/

[23] Huber+Suhner, SUCOFLEX 106, https://www.hubersuhner.com/en

[24] CST STUDIO SUITE, http://www.cst.com